

Dynamic MRI in the Rat Brain at 3.0 T for Measuring Permeability of the Blood-Brain Barrier in Glioblastoma Multiforme

Hunter R Underhill¹ and Robert C Rostomily¹

¹Neurological Surgery, University of Washington, Seattle, WA, United States

Introduction: Contrast enhancement on MRI due to blood-brain barrier (BBB) disruption is an elemental feature of glioblastoma multiforme (GBM). Measuring BBB permeability in animal models of GBM affords the opportunity to evaluate effects of therapy and identify phenotypic differences between tumors with unique genotypes. Dynamic MRI has been used to mathematically model a combination of kinetic parameters that govern BBB permeability. However, the application of dynamic MRI in small animals at 3.0 T has both physiologic and technical challenges. First, neovasculature associated with GBM lacks an intact BBB.¹ In addition, high BBB permeability coupled with relatively long intervals during dynamic scanning allows gadolinium to collect in tissue prior to the first image acquisition after bolus injection. Thus, the ability to differentiate permeability (k^{trans}), fractional plasma volume (v_p), and/or fractional volume of extravascular extracellular space (v_e), as some models have proposed,² is difficult. Second, susceptibility artifacts associated with bolus injection of gadolinium into a vessel orthogonal to the main magnetic field caused by the animal positioning necessary to accommodate solenoid coils in a 3.0 T whole-body scanner affects measurement of the arterial input function. And finally, the tissue heterogeneity characteristic of GBM may confound measurements of permeability due to variability of R_1 in the tumor. In this study, we sought to develop a dynamic MRI technique for directly measuring *in vivo* BBB permeability in a rat model of GBM at 3.0 T on a whole-body, clinical scanner.

Theory: We propose a simplification of the Brix method³ to solely extract permeability (i.e. k^{trans}) from a linearized two-compartment open model (Fig. 1). The advantages of this modified continuous infusion approach are: 1) a single parameter fit removes ambiguity of using multi-parameter models on data from tissue that are physiologically abnormal; 2) negligible susceptibility artifact due to slower rate of infusion; and 3) noise present in other methods due to the delay between bolus and initial signal acquisition is removed. The differential equations to describe the mass balance of the model (Fig. 1) are: [1] $\frac{dC_p}{dt} = K_{in} - C_p K_e - C_p k^{trans}$ and [2] $\frac{dC_t}{dt} = C_p k^{trans}$, where [1] simplifies to [3] $\frac{dC_p}{dt} = K_{in} - C_p K_e$ assuming the relative amount of gadolinium entering the tumor is negligible compared to other losses. Solving these differential equations, [2] and [3], with the initial conditions $C_p(0) = 0$ and $C_t(0) = 0$ yields: [4] $C_t(t) = k^{trans} \int_0^t C_p dt$ and [5] $C_p(t) = \frac{K_{in}}{K_e} (1 - e^{-K_e t})$, respectively. The equation for a spoiled

GRE (SPGR) sequence is:⁴ [6] $S(C_t) = GPD e^{-TE(R_2^* + R_2^* C_t)} \sin \theta \frac{1 - e^{-TR(R_1^* + R_1^* C_t)}}{1 - \cos \theta e^{-TR(R_1^* + R_1^* C_t)}}$, where G is the gain, PD is proton density, R_1^* and R_2^* are relaxivity of tissues prior to gadolinium infusion, and R_1^* and R_2^* are the relaxivities of gadolinium at 3.0 T and 37° C. Using signal enhancement [7] $E(t) = \frac{S(C_t) - S(0)}{S(0)}$ with Eq. [6] allows determination of gadolinium concentration in tissue and plasma for determination of k^{trans} from Eqs. [4] and [5] during a continuous infusion of gadolinium without dependence on G , PD , and R_2^* .

Methods: Seven adult male Wistar rats (320–380 g) were imaged two weeks after intracranial inoculation with C6 cells. Rats were anesthetized with isoflurane and imaged on a 3.0 T whole-body scanner (Philips Achieva) with a T/R head coil for RF transmission and an in-house built combined solenoid-surface coil⁵ for RF reception. Pre-contrast R_1 maps were obtained using the variable flip angle method with a 3D SPGR sequence (TR/TE = 20/2.3 ms, $\alpha = 4, 10, 20,$ and 30°). B_1 maps were acquired (3D SPGR: TR₁/TR₂/TE = 25/125/6.7, ms, $\alpha = 60$) to establish actual flip angles during parameter fitting.⁶ Twenty-two dynamic scans were obtained with a 3D SPGR sequence (TR/TE 12.3/4.5 ms, $\alpha = 18^\circ$) and $\Delta = 3.47$ ms. Coincident with the fourth dynamic scan, 0.2 mmol/kg of gadopentetate dimeglumine (Magnevist, Bayer Health Care) was infused over 10 s followed by 0.5 mL normal saline flush over 5 s. A post-contrast image was obtained 5 minutes after initiation of the gadolinium infusion. All images were acquired in the sagittal plane relative to the scanner gantry (coronal plane relative to the rat brain) with FOV = 24×24×8.25 mm and resolution 0.375×0.375×1.5 mm (zero-interpolated to 0.19×0.19×0.75 mm). Total scan time was <6 minutes. The median value of the dynamic images acquired before gadolinium infusion determined $S(0)$ in Eqn. [7] for the subsequent calculation of $E(t)$. The sagittal sinus was used for the arterial input function since the length and absence of tortuosity minimized effects of partial voluming associated with through-plane resolution. Parameters (R_1 , B_1 , and k^{trans}) were calculated using both an ROI and voxel-based approach. Nonlinear least squares fitting for Eqn. [4] and [5] was performed with a Levenberg–Marquardt algorithm.

Results: The rate of gadolinium infusion enabled 7-8 dynamic data points for calculation of k^{trans} . Representative data points and fitted curves from the sagittal sinus, regions of a tumor with different levels of k^{trans} , and normal brain are shown in Figure 2. Voxel-based reconstructions of pre- and post-contrast R_1 -maps and k^{trans} maps are shown in Figure 3. A comparison of voxel-based reconstructions of k^{trans} within tumors using R_1 -maps were significantly lower than when a single fixed value of R_1 was utilized (0.53 ± 0.27 vs. 0.69 ± 0.40 min⁻¹, respectively; $p < 0.001$). Similarly, k^{trans} was significantly lower using voxel-based flip angle correction with B_1 -maps during determination of R_1 -maps and Eqn. [6] compared to no flip angle correction (0.53 ± 0.27 vs. 0.59 ± 0.30 min⁻¹, respectively; $p < 0.001$). Within the tumors, there was a significant association between k^{trans} and post-contrast R_1 , although the correlation was mild (Pearson's $r = 0.39$, $p < 0.001$).

Conclusions: The proposed simplification of the Brix method provides voxel-based determinations of k^{trans} in an animal model of GBM using a 3.0 T, whole-body, clinical scanner. The methodology accounts for variations in R_1 associated with tissue variability and also for B_1 heterogeneity that may be present when imaging at increased field-strengths. Not accounting for either of these parameters leads to significant differences of k^{trans} in GBM. Voxel-based k^{trans} maps identified both high and low areas of permeability within the tumor, which was contrary to post-contrast R_1 -maps that appeared relatively homogenous. Areas of post-contrast enhancement on R_1 -maps with low values on k^{trans} -maps may be a consequence of gadolinium diffusion from nearby tissue rather than locally increased BBB permeability. The technique described herein may be beneficial for measuring k^{trans} to effectively characterize permeability of the BBB in animal models of GBM during natural history studies and to monitor response to therapy.

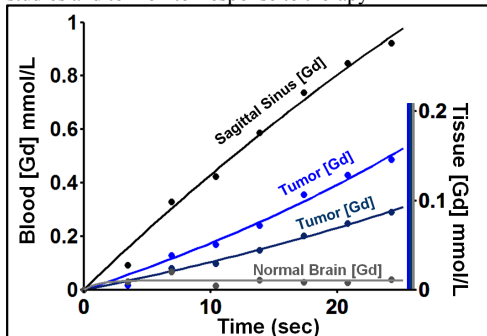


Figure 2. ROI-based [Gd] in the sagittal sinus (black; left y-axis) subsequently used to determine [Gd] in ROI from tissues (right y-axis): two different regions of tumor, (light and dark blue) and normal brain (gray).

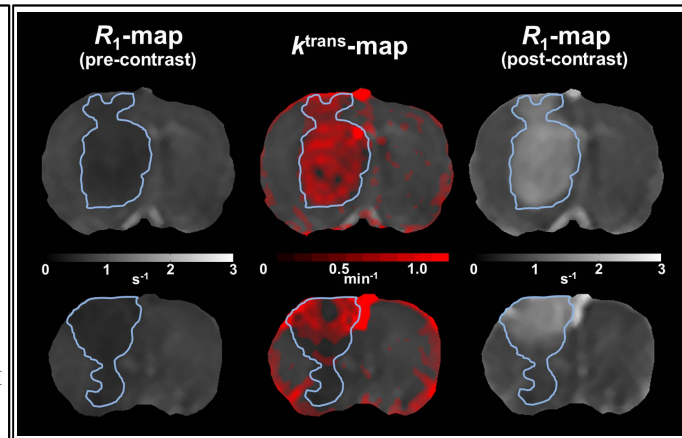


Figure 3. Voxel-based comparison of parametric maps in the coronal plane of two different rats with a GBM tumor. Pre-contrast R_1 -maps were used to outline the tumor (blue line). Notice variability in the k^{trans} -map (top row), but relatively homogenous appearance of enhancement in the post-contrast R_1 -map. In contrast, the tumor in the bottom row exhibits a different phenotype with variable to absent BBB disruption in the tumor.

References: 1. Jain *Nat Rev Neurosci* 2007;8:610-22 2. Tofts *JMRI* 1999;10:223-32 3. Brix *J Comp Assisted Tomography* 1991;15:621-8 4. Tofts *MRM* 1995;33:564-8 5. Underhill *MRM* 2010;64:883-92 6. Yarnykh *MRM* 2007;57:192-200